ACS APPLIED MATERIALS & INTERFACES

RESEARCH ARTICLE

www.acsami.org

Sub-micrometer-sized Graphite As a Conducting and Catalytic Counter Electrode for Dye-sensitized Solar Cells

Ganapathy Veerappan, Karunagaran Bojan, and Shi-Woo Rhee*

System on Chip Chemical Process Research Center, Department of Chemical Engineering, Pohang University of Science and Technology (POSTECH), Pohang, 790-784, Korea

ABSTRACT: Sub-micrometer-sized colloidal graphite (CG) was tested as a conducting electrode to replace transparent conducting oxide (TCO) electrodes and as a catalytic material to replace platinum (Pt) for I_3^- reduction in dye-sensitized solar cell (DSSC). CG paste was used to make a film via the doctor-blade process. The 9 μm thick CG film showed a lower resistivity (7 Ω/□) than the widely used fluorine-doped tin oxide TCO (8−15 Ω/□). The catalytic activity of this graphite film was measured and compared with the corresponding properties of Pt. Cyclic voltammetry and electrochemical impedance spectroscopy studies clearly showed a decrease in the charge transfer resistance with the increase in the thickness of the graphite layer from 3 to 9 μm. Under 1 sun illumination (100 mW cm^{-2}, AM 1.5), DSSCs with submicrometer-sized graphite as a catalyst on fluorine-doped tin oxide TCO showed an energy conversion efficiency greater than 6.0%, comparable to the conversion efficiency of Pt. DSSCs with a graphite counter electrode (CE) on TCO-free bare glass showed an energy conversion efficiency greater than 5.0%, which demonstrated that the graphite layer could be used both as a conducting layer and as a catalytic layer.

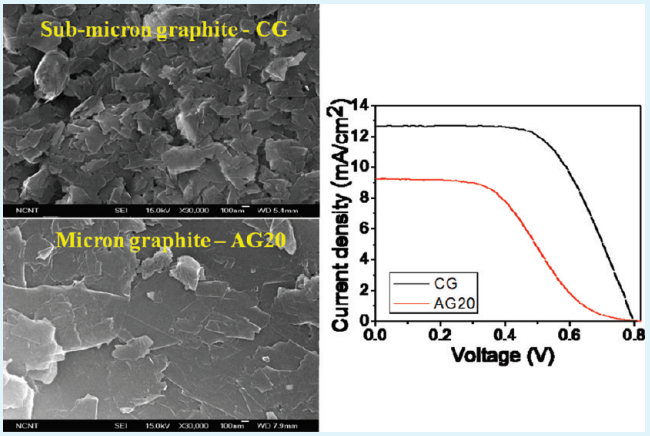

KEYWORDS: dye-sensitized solar cell, graphite layer, catalytic activity, counter electrode, conducting catalytic electrode, charge transfer resistance

1. INTRODUCTION

Dye-sensitized solar cells (DSSCs) have emerged as a viable alternative to solid-state silicon solar cells because of their low cost and high energy conversion efficiency.[1] These cells normally consist of transparent conducting oxide (TCO) films on a glass substrate, a wide band gap semiconductor, a ruthenium based dye, a redox electrolyte solution and a platinum (Pt) coated counter electrode. The working mechanism involves the ultrafast injection of electrons from the photoexcited state of the dye to the conduction band of the semiconductor. The counter electrode (CE) acts as an electron carrier from the external circuit to the redox electrolyte. The Iodide (I^-) ions present in the redox electrolyte reduce the oxidized dye and the resultant tri-iodide (I_3^-) ions are reduced back to I^- ions at the CE.[2] Commonly, fluorine doped tin oxide (FTO) coated glass is used as a substrate and Pt is used as a catalyst for the tri-iodide reaction on a standard CE material in DSSCs. Despite the good catalytic activity of platinum CE in DSSCs, the high cost, poor stability in corrosive electrolytes, and high processing temperatures necessitate the development of alternative CE materials. FTO glass substrates have several limitations, such as high cost, high sheet resistance, and brittleness, which make them nonviable for flexible large-scale DSSCs.[3−6] To develop large-scale applications, an abundant-material is preferred. In the recent past, various carbon materials have been described, including carbon nanotubes (CNTs),[7−10] activated carbon, graphite,[11] nanocarbon,[12] carbon black,[9,13] conducting polymers,[14,15] and graphene.[16] High catalytic activities have been achieved, using carbon black or carbon black mixed with graphite as an efficient CE.[17] Although many reports have described carbon materials, the use of graphite alone as an efficient CE catalyst or as a conducting layer on bare glass substrate has not been described.

Pt coated TCO used in DSSCs is responsible for more than 40% of the total device cost,[4] which makes it nonviable for large scale applications. Recent attempts at using TCO-free counter electrodes based on flexible graphite sheets[5] and polymer-based substrates[6] showed low conversion efficiencies. Graphite is an interesting catalyst and conducting layer material, and it is abundantly available in nature at low-cost. In general, graphitic materials, such as CNTs and graphite, have basal and edge planes. Basal planes exhibit slow electron transport whereas edge planes exhibit fast electron transport.[18] Graphite particles of large size

Received: December 7, 2010
Accepted: February 7, 2011
Published: February 25, 2011

and low surface area show very poor catalytic activity as CE materials.[11,19] This is because large graphite particles have fewer edge planes (or more basal planes), which slows the rate of I_3^- reduction due to the high charge transfer resistance (R_{CT}). The high R_{CT} has a negative influence on the fill factor (FF) and shows poor energy conversion efficiency (η).

In this paper, we report the use of submicrometer size graphite (700−900 nm) as both a conducting counter electrode and a CE catalyst in DSSCs. These graphite particles present abundant edge planes and good conductivity, which enhance the catalytic effects (low R_{CT} and higher FF). Figure 1a shows the graphite structure and highlights the stacking arrangements of the basal and edge planes. Panels b and c in Figure 1 show schematic diagrams of the graphite samples used here, namely, AG20 (micrometer graphite) and CG (submicrometer graphite). As seen in Figure 1b, AG20 graphite has fewer edge planes, so it may yield a low catalytic I_3^- reduction rate. In contrast, CG graphite (Figure 1c) has an abundance of edge planes which increase the I_3^- reduction rate and improve the conductivity.[18] Panels d and e in Figure 1 depict the reduction reaction on TCO-graphite CE in DSSCs and on TCO free CE.

2. EXPERIMENTAL SECTION

TiO_2 Photo Electrode Preparation. A semitransparent TiO_2 nanoparticulate layer 12 μm in thickness was prepared by doctor-blading a paste of TiO_2 nanoparticles (Ti-Nanoxide HT/SP from Solaronix) on to the ultrasonically cleaned fluorine doped tin oxide (FTO, 8 Ω/□) glass substrates. After drying at 120 °C, the electrodes were annealed at 500 °C for 30 min in air and subsequently immersed in a 0.3 mM solution of N719 dye in a mixture of acetonitrile/tert-butanol (volume ratio 1:1) for 24 h. Dye soaked electrodes were removed from the dye solution, rinsed with ethanol, and then dried under a high-purity nitrogen stream.

Graphite Counter Electrode Preparation. Graphite electrodes were deposited by screen-printing on a TCO coated glass, and by doctor-blading method on a bare glass substrate. The commercial colloidal graphite paste (CG) was purchased from Electron Microscopy Sciences and had a particle size range of 700−900 nm. The graphite layer was deposited on a cleaned FTO glass substrate by screen-printing, and

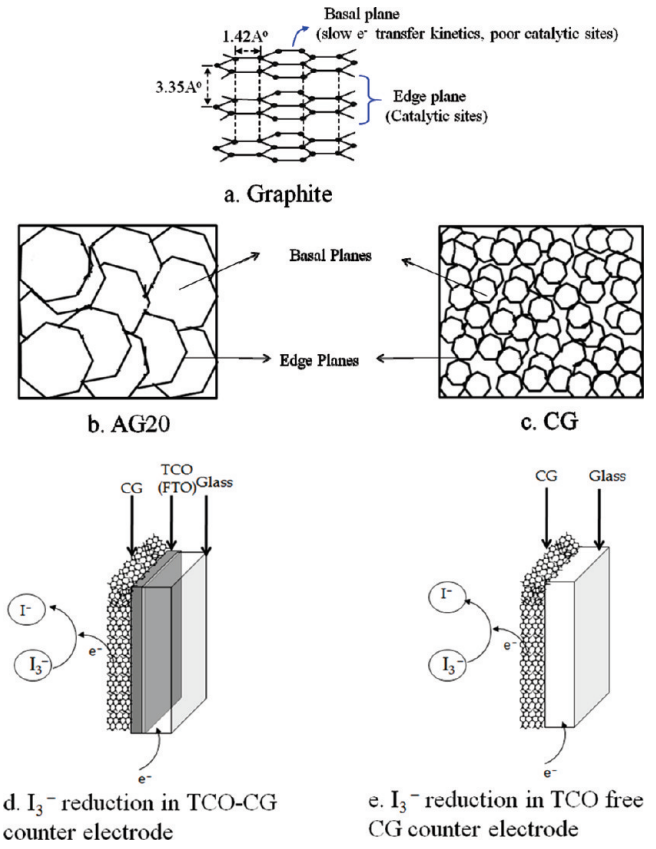

Figure 1. Schematic diagram of graphite and reduction reaction in the graphite counter electrode, (a) graphite structure, (b) 20 μm graphite particle (AG20), (c) submicrometer graphite (CG), (d) I_3^- reduction in TCO-CG counter electrode, and (e) I_3^- reduction in TCO free CG counter electrode.

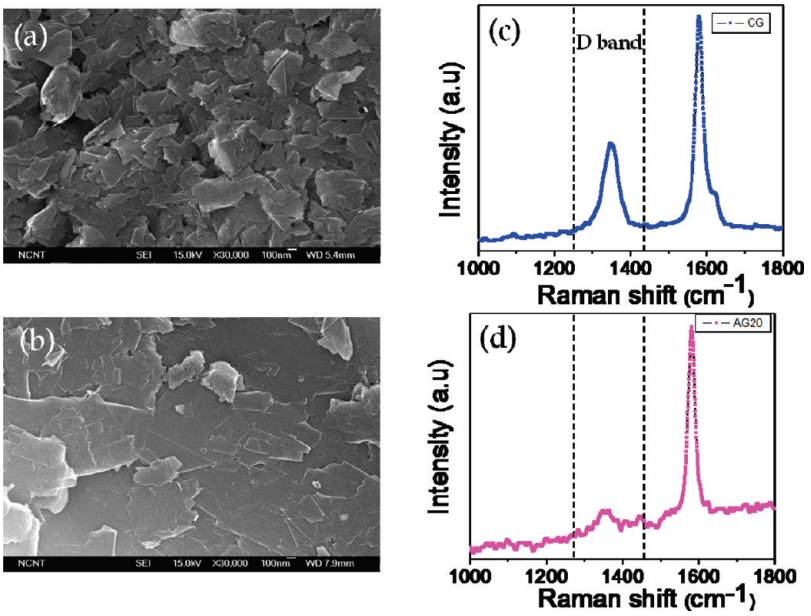

Figure 2. SEM surface images and Raman spectra of graphite samples (a, c) CG and (b, d) AG20.

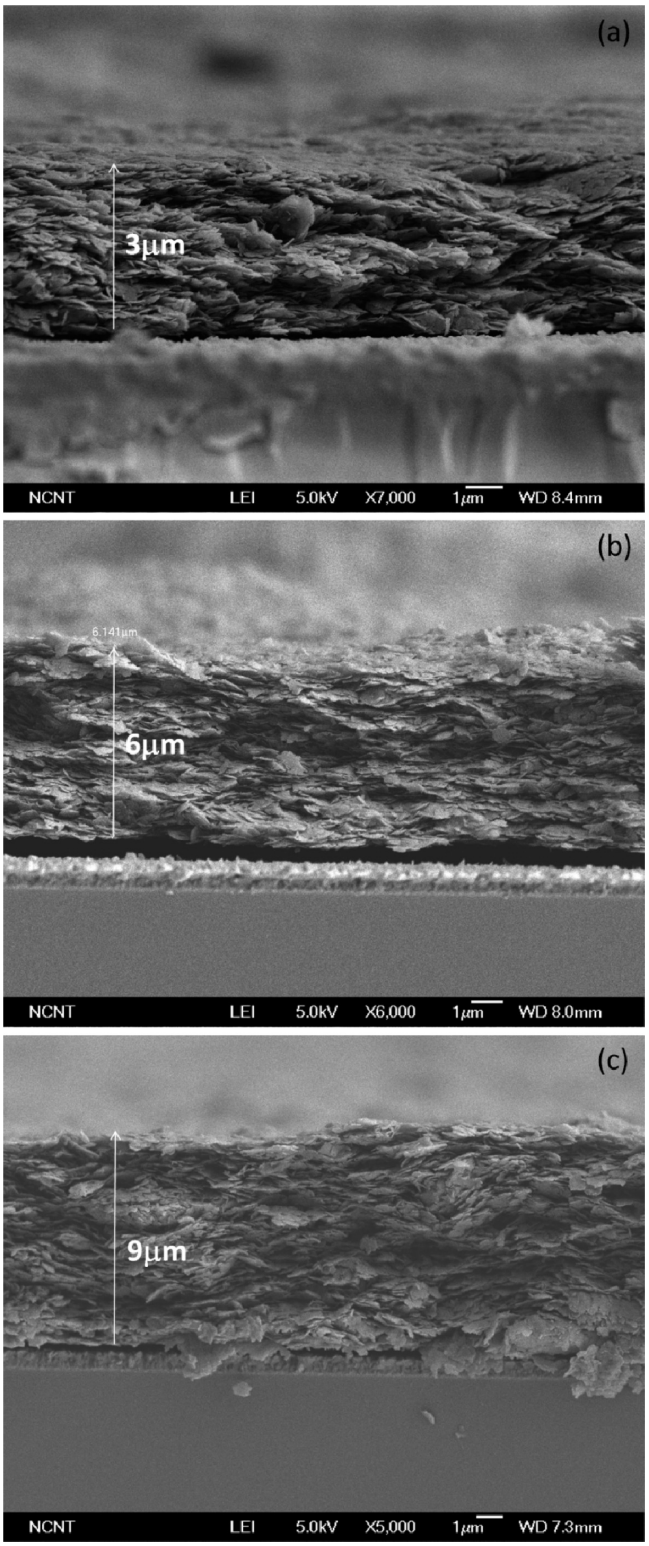

Figure 3. Cross-sectional SEM images of graphite layer with different thickness: (a) CG-a, (b) CG-b, (c) CG-c.

the thickness of the layer was controlled by the number of screen-printing processes. Each printing process gave a film 3 μm thick, and three different samples, CG-a (3 μm), CG-b (6 μm), and CG-c (9 μm) were tested. For comparison, larger graphite particles were used, and the paste was prepared using Aldrich graphite (AG20) particles (particle size

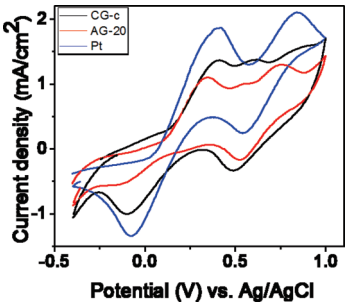

Figure 4. Cyclic voltammograms obtained at a scan rate of 50 mV s^{-1} for the reduction of I_2^-/I_3^- with the various electrode materials.

>20 μm), distilled water, and an organic binder. One gram of a carboxylmethyl cellulose (CMC) sodium salt (Sigma Aldrich, viscosity 50−200 cP) was dissolved in 39 mL of distilled water, and 1.5 g of graphite powder was added to the binder solution. The mixture was ground using a mortar and pestle. The resulting paste was coated onto the cleaned FTO glass substrate by doctor-blading to give a thickness of 20 μm. Both the CG and AG20 graphite CEs were annealed at 300 °C for 30 min. Colloidal graphite (CG) deposited directly on a glass substrate will be called in this work as a TCO free CE. It was prepared with doctor-blading CG on a glass substrate followed by sintering at 300 °C for 30 min. The film thickness was 8−9 μm. For comparison, a traditional Pt CE was also prepared by screen-printing (paste from Solaronix) on the FTO glass substrate followed by annealing at 450 °C for 30 min.

Cell and Characterization. A 60 μm thick hot melt ionomer film (Surlyn, SX1170−60 from Solaronix) was sandwiched between the TiO_2 working electrode and a Pt or graphite CE by heating at 110 °C for a few seconds. The space between the electrodes was filled with liquid electrolyte consisting of 0.6 M 1-butyl-3-methyl imidazolium iodide, 0.03 M I_2, 0.1 M guanidinium thiocyanate, and 0.5 M 4-tertbutylpyridine in a solvent mixture of acetonitrile and valeronitrile (volume ratio, 85:15). After electrolyte injection, the hole was sealed with Surlyn and a thin cover glass.

To measure the R_{CT}, we prepared symmetric cells by stacking two graphite or Pt electrodes facing each other with a 60 or 120 μm thick Surlyn spacer.[20] The symmetric cells were then filled with the liquid electrolyte solution described above.

Current−voltage ($I-V$) characteristics of the DSSCs were measured using a solar simulator equipped with a 300 W xenon lamp. The power of the simulated light was calibrated to give AM 1.5, 100 mW cm^{-2}, using a standard Si solar cell. I−V curves were obtained by applying an external bias to the cell and measuring the photocurrent generated using a Keithley model 2400 digital source meter. The electrochemical characteristics of various catalytic materials were measured by cyclic voltammetry (CV) and electrochemical impedance spectroscopy (EIS). CV measurements were carried out in an acetonitrile solution containing 10 mM LiI, 1 mM I_2, and 0.1 M $LiClO_4$ with a scan rate of 50 mV s^{-1}. EIS measurements were carried out in the dark at room temperature in over the frequency range from 100 mHz to 100 kHz. The electrochemical parameters were derived from the AC impedance spectra using the "Zsimpwin" impedance analysis software.

3. RESULTS AND DISCUSSION

The surface morphology and Raman spectra of the graphite films are presented in Figure 2. The SEM surface morphological images a and b in Figure 2 clearly revealed that CG had more edge planes, i.e., a higher number of catalytic sites,[18] than AG20. The Raman spectra (Figure 2c, d) showed two bands, the D band at 1355 cm^{-1} and the G band at 1579 cm^{-1}. The D band usually

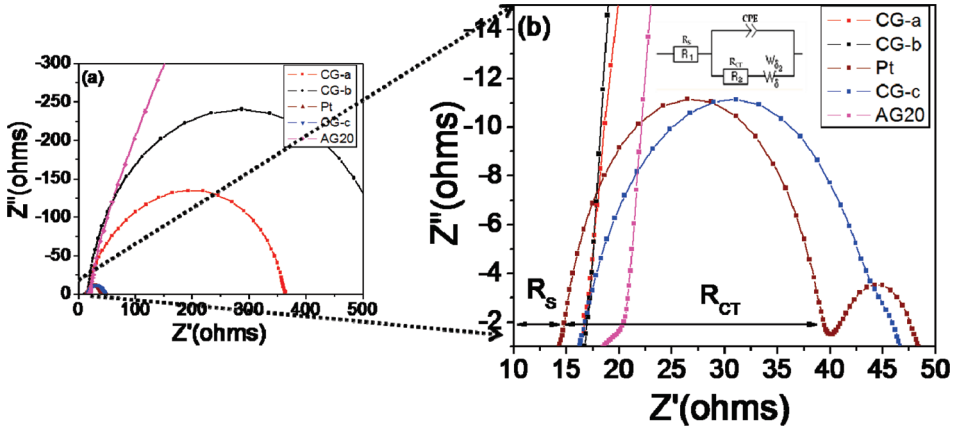

Figure 5. Nyquist plot of graphite and platinum symmetric cells. Equivalent circuit diagram for graphite is given in the inset.

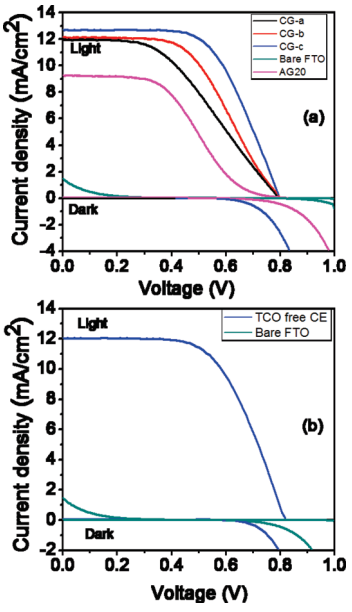

Figure 6. (a) Photocurrent−voltage characteristics of CG, bare FTO, AG20 counter electrode based DSSCs, and (b) photocurrent−voltage characteristics of TCO free CE, and bare FTO.

indicates the structure, size, and defects of the carbon material.[21] Defects are advantageous for producing an effective catalytic activity.[8] The D band was strong in the CG sample due to the smaller particle size and increased number of defect sites in the edge plane.[21,22] In AG20, the D band was much smaller because AG20 graphite was composed of larger particles and the edge planes had smaller defects. Figure 3 shows cross-sectional SEM images of CG graphite layers of different thicknesses on FTO bare glass substrates. The CG graphite thickness was increased by repeated screen-printing, and each layer was dried before depositing the next layer. The SEM cross-sectional images given in Figure 3 clearly show the thickness increase in CG graphite after repeated coating applications. The single-layer doctor-bladed AG20 thickness was ~20 μm. With bigger particle size, it is difficult to make a thin layer and we did not make a film with different thickness with AG20 paste.

CV is an important and efficient tool for analyzing ion diffusivity and the catalytic mechanism acting in an electrochemical system.[23] Figure 4 shows the CVs for I_2/ I_3^- reduction obtained using various counter electrode materials (versus Ag/AgCl) in acetonitrile at a scan rate of 50 mVs^{-1}. The two anodic peaks obtained from the CV curves corresponded to the oxidation of iodide to tri-iodide 1 and the cathodic peak corresponded to the reduction of tri-iodide 2.[23,11]

$$3I^- \rightarrow I_3^- + 2e^- \text{(oxidation)} \quad (1)$$

$$I_3^- + 2e^- \rightarrow 3I^- \text{(reduction)} \quad (2)$$

The oxidation and reduction peaks observed in the CG-c were comparable to those of the Pt electrode, which indicated the possibility of achieving similar electrocatalytic behavior for small-size high-surface-area graphite particles. Electrocatalytic behavior in these systems relies on the presence of edge planes in the submicrometer-size graphite. AG20 showed a much lower current density, indicating a poor reduction rate compared to CG-c and Pt electrodes. This coincided with the charge transfer resistance R_{CT} obtained from the EIS measurements, discussed-below. High-surface-area edge planes in the CG-c increased the electrocatalytic activity.

In general, EIS analysis and equivalent circuit fitting of DSSCs provide an estimate for the internal resistance in the cells.[24−30] A higher internal resistance in a device decreases the FF and J_{SC}. The internal resistance of DSSCs mainly arises from charge transfer processes at the CEs, the sheet resistance (R_S) of the substrates, the electron transfer at the TiO_2/dye/electrolyte interface, and ion transport within the electrolyte.[24] To check the catalytic behavior of the graphitic electrode, R_{CT} of the symmetric cells were measured using EIS. Figure 5 shows the Nyquist plot of the Pt and graphite symmetric cells. Figure 5b shows an enlarged version of Figure 5a, which clearly shows the high frequency region of the CG-c and Pt electrodes. R_{CT} and R_S were calculated using equivalent circuit fitting. The first semicircle in the high frequency region arose from the catalytic property, the charge transfer resistance (R_{CT}) at the counter electrode. The second semicircle at the low frequency arose from Nernstian diffusion in the electrolyte.[25−27] The R_{CT} of a single electrode is half of the real component of the impedance determined from the high-frequency semicircle. R_{CT} was found by fitting the impedance data using the "Zsimpwin" software based on equivalent circuit modeling of symmetric cells.[20] The calculated R_{CT} of CG-c (5.0 Ωcm^{-2}) was very close to that calculated for the conventional Pt electrode (4.5 Ωcm^{-2}),

Table 1. Current−Voltage Parameters of the DSSCs with Platinum, Graphite, and TCO-Free CE Measured under 1 sun Illumination

counter electrode catalyst	R_{CT} (Ω cm^{-2})	J_{SC} (mA cm^{-2})	V_{OC} (V)	*FF* (%)	η (%)
bare FTO		1.4 ± 0.21	0.681 ± 0.01	0.05 ± 0.001	0.04 ± 0.004
AG20	24.2 ± 0.1	9.6 ± 0.27	0.807 ± 0.01	40.9 ± 0.02	3.2 ± 0.24
CG-a	18.4 ± 0.2	11.9 ± 0.21	0.795 ± 0.01	44.0 ± 0.02	4.1 ± 0.22
CG-b	12.6 ± 0.1	12.1 ± 0.35	0.801 ± 0.01	52.4 ± 0.02	5.0 ± 0.23
CG-c	5.0 ± 0.3	12.7 ± 0.34	0.794 ± 0.01	62.0 ± 0.03	6.2 ± 0.24
Pt	4.5 ± 0.2	13.0 ± 0.52	0.804 ± 0.01	65.0 ± 0.04	6.8 ± 0.34
TCO free CE		12.0 ± 0.41	0.818 ± 0.01	60.0 ± 0.02	5.9 ± 0.247

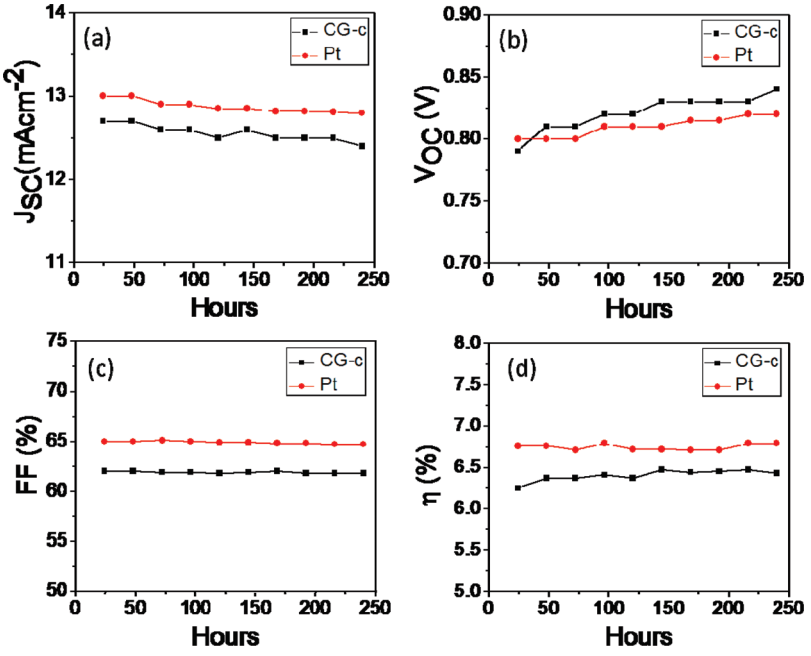

Figure 7. Short time evaluation of $I-V$ parameters in DSSC with CG-c graphite. (a) open-circuit voltage, V_{OC}; (b) short-circuit current density, J_{SC}; (c) fill-factor, FF; and (d) energy conversion efficiency, η.

whereas CG-a, CG-b, and the R_{CT} of AG20 was higher than that of CG-c due to a smaller number of catalytic sites. The sheet resistance (R_S) of the CG electrode was slightly higher than that of the Pt electrode, possibly due to the larger thickness and the rougher CG and AG20 film surfaces.[13,31,32] Therefore, the CG devices displayed lower values for the FF, J_{SC}, and lower efficiency.[24]

The dark $I-V$ characteristics of the DSSCs prepared using each type of graphite CE is shown in Figure 6a. The dark current onset of all devices began at ~500 mV. The CG dark current was higher than that of AG20 due to the higher catalytic activity. The tri-iodide produced by the dye-sensitized TiO_2 electrodes was generally reduced at the CE, and the reduction of I_3^- ions was slower at the AG20 CE than at the CG CE. As a result, AG20 and bare FTO showed smaller dark currents.[33]

Figure 6a shows the photovoltaic performance of the bare FTO with very poor FF, J_{SC} and V_{OC}, which clearly addresses the need for an electro catalyst in DSSCs. The conversion efficiency of the graphitic CE was comparable to that of the Pt CE when CG-c was used. The photovoltaic performances of the CE materials are summarized in Table 1. The CG CE showed similar values for J_{SC} and V_{OC}, with variations in the FF alone. CG graphite showed an improved FF when the thickness of CE was increased. A stacking arrangement involving a greater number of edge planes in the CG-c (thickness ~of 9 μm) increased the rate of I_3^- reduction compared with CG-a (thickness ~of 3 μm) and CG-b (thickness ~of 6 μm). The effects of the micrometer-size graphite (AG20) particle size on device performance were examined. Even very thick micrometer-size graphite films, were not able to improve the catalytic activity, and AG20 showed a much lower FF, poor device performance, and poor catalytic activity toward the reduction of iodine.[34] Recent studies have suggested that edge planes are responsible for fast electron transfer kinetics and electrocatalytic properties in carbon materials.[18] AG20 has near-perfect and atomically smooth basal plane walls so those electrons transfer kinetics are limited.

Figure 6b shows the $I-V$ characteristics of the TCO-free CE and the corresponding values are listed in Table 1. DSSCs made with the bare FTO performed poorly because of the impotency of FTO substrate for I_3^- reduction. The TCO-free graphite substrate showed a low resistivity of 7$\Omega/\square$, as measured by the four-point probe method. The catalytic properties of CG graphite improved for thicker CG graphite films. The optimal material for both catalytic activity and conductivity was found

to be CG-c. A comparison of TCO with the catalyst CE in DSSCs showed that the TCO-free CE decreases J_{SC} and FF. J_{SC} was decreased from 12.7 mA cm^{-2} to 12.0 mA cm^{-2}, and the FF decreased from 62% to 60%. These changes were attributed to the slightly higher sheet resistance in the CG-c graphite than in the FTO substrates, which was also observed by EIS. For large-scale applications, small decreases in the efficiency are acceptable, because graphite CE may decrease the cost of DSSCs by 40%.

Figure 7 shows the stability data for the CG graphite CE.[8] One of the most important considerations for the CE materials is stability in the redox electrolyte. The CG graphite CE showed promising stability, even after 250 h of operation. The short-term evaluation test, revealed only small decreases in J_{SC}, V_{OC} changed moderately from 0.7 to 0.84 V, and the FF did not change significantly. An increase in V_{OC} and a decrease in J_{SC} resulted either from the shift in the conduction band of the TiO_2 toward negative values or the I^-/I_3^- redox energy level shift to the positive values.[10] The stability of Pt showed similar performance which was given in the Figure 7. In general, the stability was measured using a light soaking test instrument, although here we used an ordinary room temperature measurement with a standard solar simulator. The performance degradation properties will be investigated further using a standard testing instrument. The overall performance of the DSSCs made with CG graphite showed promising stability and can be a successful replacement material for Pt in large-scale applications.

4. CONCLUSION

We have successfully employed submicrometer-size colloidal graphite (CG) as an efficient counter electrode catalyst for triiodide reduction in DSSCs. The high conductivity of submicrometer graphite suggests that TCO-free DSSCs may be developed using CG. Advantageously, CG may act dually as a substrate and an electro-catalyst so that it may successfully replaced both TCO and Pt. The charge transfer resistance and device performance of 9 μm thick submicrometer graphite layers as a counter electrode showed promising results. The high catalytic effects mainly arose from the edge planes in the submicrometer graphite. The low-cost TCO-free graphite catalytic counter electrode optimized in the present work showed an energy conversion efficiency of 85% the conversion efficiency of conventional Pt-coated TCO counter electrode.

AUTHOR INFORMATION

Corresponding Author

*E-mail: srhee@postech.ac.kr. Tel: 82-54-279-2265. Fax: 82-54-279-8619.

ACKNOWLEDGMENT

This research was supported by the Korea Science and Engineering Foundation (KOSEF) through the National Research Laboratory Project and the nano fusion program of POSCO. G.V. is thankful to Jung Min Kim and Dong Jin Yun for the help in the measurements and Hyunjin Park at NCNT for supporting SEM analysis.

REFERENCES

(1) O'Regan, B.; Grätzel, M. *Nature* **1991**, *353*, 737–740.
(2) Gregg, B. A. *J. Phys. Chem. B* **2003**, *107*, 4688–4698.
(3) Okada, K.; Matsui, H.; Kawashima, T.; Ezure, T.; Tanabe, N. *J. Photochem. Photobiol. A* **2004**, *164*, 193–198.
(4) Kroon, J. M.; Bakker, N. J.; Smit, H. J. P.; Liska, P.; Thambi, K. R.; Wang, P.; Zakeeruddin, S. M.; Grätzel, M.; Hinsch, A.; Hore, S.; Wurfel, U.; Sastrawan., R.; Durrant, J. R.; Palomares, E.; Pettersson, H.; Gruszecki, T.; Walter, J.; Skupien, K.; Tulloch, G. E. *Prog, Photovlot: Res. Appl.* **2007**, *15*, 1–18.
(5) Chen, J.; Li, K.; Luo, Y.; Guo, X.; Li, D.; Deng, M.; Huang, S.; Meng, Q. *Carbon* **2009**, *47*, 2704–2708.
(6) Lee, K. S.; Lee, H. K.; Wang, D. H.; Park, N. G.; Lee, J. Y.; Park, O. O.; Park, J. H. *Chem Commmun.* **2010**, *46*, 4505–4507.
(7) Suzuki, K.; Yamaguchi, M.; Kumagai, M.; Yanagida, S. *Chem. Lett.* **2003**, *32*, 28–29.
(8) Lee, W. J.; Ramasamy, E.; Lee, D. Y.; Song, J. S. *Appl. Mater. Inter.* **2009**, *1*, 1145–1149.
(9) Zhu, H.; Zeng, H.; Subramanian, V.; Masarapu, C.; Hung, K.-H.; Wei, B. *Nanotechnology* **2008**, *19*, 465204–5.
(10) Sayer, R. A.; Hodson, S. L.; Fisher, T. S. *J. Sol. Energy Eng.* **2010**, *132*, 021007–4.
(11) Imoto, K.; Takahashi, K.; Yamaguchi, T.; Komura, T.; Nakamura, J.; Murata, K. *Sol. Energy Mater. Sol. Cells* **2003**, *79*, 459–469.
(12) Ramasamy, E.; Lee, W. J.; Lee., D. Y.; Song, J. S. *Appl. Phys. Lett.* **2007**, *90*, 173103–3.
(13) Murakami, T. N.; Ito, S.; Wang, Q.; Nazeeruddin, M. K.; Bessho, T.; Cesar, I.; Liska, P.; Humphry- Baker, R.; Comte, P.; Pechy, P.; Grätzel, M. *J. Electrochem. Soc.* **2006**, *153*, A2255–A2261.
(14) Saito, Y.; Kitamura, T.; Wada, Y.; Yanagida, S. *Chem. Lett.* **2002**, *31*, 1060–1061.
(15) Xia, J. B.; Masaki, N.; Jiang, K. J.; Yanagida, S. *J.Mater. Chem.* **2007**, *17*, 2845–2850.
(16) Mayhew, J.D. R.; Bozym, D. J.; Punckt, C.; Aksay, I. A. *ACS Nano* **2010**, *4*, 6203–6211.
(17) Huang, Z.; Liu, X.; Li, K.; Li, D.; Luo, Y.; Li, H.; Song, W.; Chen, L.; Meng, Q. *Electrochem. Commun.* **2007**, *9*, 596–598.
(18) Banks, C. E.; Davies, T. J.; Wildgoose, G. G.; Compton, R. G. *Chem. Commun.* **2005**, *7*, 829–841.
(19) Gagliradi, S.; Giorgi, L.; Giorgi, R.; Lisi, N.; Makaris, Th. D.; Salernitano, E.; Rufoloni, A. *Superlattices Microstruct.* **2009**, *46*, 205–208.
(20) Papageorgiou, N.; Maier, W. F.; Grätzel, M. *J. Electrochem. Soc.* **1997**, *144*, 876–884.
(21) Reich, S.; Thomsen, C. *Philos. Trans. R. Soc. London, Ser. A* **2004**, *362*, 2271–2288.
(22) Tuinstra, F.; Koenig, J. L. *J. Chem. Phys.* **1970**, *53*, 1126–1130.
(23) Wei, T.- C.; Wan, C.-C.; Wang, Y.-Y.; Chen, C.-M.; Shiu, H.-S. *J. Phys. Chem. C* **2007**, *111*, 4827–4853.
(24) Han, L.; Koide, N.; Chiba, Y.; Islam, A.; Komiya, R.; Fuke, N.; Fukui, A.; Yamanaka. *Appl. Phys. Lett.* **2005**, *86*, 213501–3.
(25) Santiago, F. F.; Bisquert, J.; Palomares, E.; Otero, L.; Kuang, D.; Zakeeruddin, S. M.; Grätzel, M. *J. Phys. Chem. C* **2007**, *111*, 6550–6560.
(26) Ganapathy, V.; Karunagaran, B.; Rhee, S.-W. *J. Power Sources* **2010**, *195*, 5138–5143.
(27) Hauch, A.; Georg, A. *Electrochim. Acta* **2001**, *46*, 3457–3466.
(28) Wang, Q.; Moser, J. E.; Gratzel, M. *J. Phys. Chem. B* **2005**, *109*, 14945–14953.
(29) Adachi, M.; Sakamoto, M.; Jiu, J.; Ogata, Y.; Isoda, S. *J. Phys. Chem. B* **2006**, *110*, 13872–13880.
(30) Li, G.-R; Wang, F.; Jiang, W.-W.; Gao, X.-P.; Shen, -P.W. *Angew. Chem., Int. Ed.* **2010**, *49*, 3653–3656.
(31) Jiang, Q. W.; Li, G. R.; Liu, S.; Gao, X. P. *J. Phys. Chem. C* **2010**, *114*, 13397–13401.
(32) Joshi, P.; Zhang, L.; Chen, Q.; Galipeau, D.; Fong, H.; Qiao, Q. *Appl. Mater. Inter* **2010**, *2*, 3572–3577.
(33) Ito, S.; Liska, P.; Comte, P.; Charvet, R.; Pechy, P.; Bach, U.; Mende, L. S.; Zakeeruddin, S. M.; Kay, A.; Nazeeruddin, M. K.; Gratzel, M. *Chem. Commun.* **2005**, *34*, 4351–4353.
(34) Trancik, J. E.; Barton, S. C.; Hone, J. *Nano Lett.* **2008**, *8*, 982–987.